Journal of The Electrochemical Society, 2023 **170** 010527

From Lab to Manufacturing Line: Guidelines for the Development and Upscaling of Aqueous Processed NMC622 Electrodes

Iratxe de Meatza,[1,2,z] Idoia Urdampilleta,[1,3] Iker Boyano,[1] Iker Castrillo,[1] Imanol Landa-Medrano,[1,3] Susan Sananes-Israel,[1] Aitor Eguia-Barrio,[1] and Verónica Palomares[2]

[1]*CIDETEC Basque Research and Technology Alliance (BRTA), Paseo Miramon 196,20014 Donostia-San Sebastian, Spain*
[2]*Department of Organic and Inorganic Chemistry, University of the Basque Country (UPV/EHU), 48080 Bilbao, Spain*
[3]*Department of Applied Chemistry, University of the Basque Country (UPV/EHU), 20018 Donostia-San Sebastian, Spain*

Lithium-ion batteries (LIBs) have facilitated the transition to a more sustainable energy model. Paradoxically, current high energy cathodes are industrially processed using organic solvents, which are deleterious for the environment. In this work, $LiNi_{0.6}Mn_{0.2}Co_{0.2}O_2$ (NMC622) high-energy cathode electrode was prepared at laboratory scale following a more environmentally friendly aqueous route. Several steps in the preparation of the electrodes (such as the drying temperature, drying air flux or pH buffering) were thoroughly optimized to enhance the quality of the water-processed electrodes. Afterwards, the recipe developed at laboratory scale was upscaled to a semi-industrial electrode coating line, to analyze the viability of the developed processing conditions into a realistic electrode manufacturing environment. The electrodes obtained were tested in full coin cells using graphite-based anodes as counter electrodes. Interestingly, the cycling performance of the cells based on water-processed electrodes was higher than that of organic-processed ones. It is evidenced that it is possible to manufacture electrodes for high energy density LIBs following environmentally friendly, cheaper, and industrially implementable electrode processing methods with no-penalty in the electrochemical performance.
 [DOI: 10.1149/1945-7111/acb10d]

Manuscript submitted November 2, 2022; revised manuscript received December 27, 2022. Published January 24, 2023. *This paper is part of the JES Focus Issue on Selected Papers from IMLB 2022.*

Supplementary material for this article is available online

Lithium-ion batteries (LIBs) have been extensively applied in a wide spectrum of energy storage applications ranging from personal portable electronic devices to satellites due its maturity among the different battery technologies available in the market.[1–4] Despite the immense success and continuous development of the electric vehicles (EVs), there are still some technical challenges that need to be addressed to compete with internal combustion engine vehicles. These account for longer cycle life (>500 cycles) and calendar life (>10 years), and stabler performance at temperatures ranging from −30 °C to 52 °C.[5–8]

Another key requirement is the reduction of the production costs of LIBs, which are currently about 250 \$ kWh^{-1}, to below 125 \$ kWh^{-1}.[5,9] In particular, the 39% of the total energy consumption of the fabrication of the $LiMn_2O_4$/graphite based batteries used in the Nissan Leaf electric cars is related to the production of the cathodes.[10] A possible approach for a simultaneous drastic decrease in the electrode fabrication costs and the environmental impact of the fabrication of LIBs could be replacing the current organic solvent-based processing of the electrode by a cheaper and greener aqueous processing. In the state-of-the-art fabrication of electrodes, a volatile solvent N-methylpyrrolidone (NMP) is employed to dissolve the state-of-the-art binder in positive electrodes: polyvinylidene-fluoride (PVDF).[11] The use of this highly toxic solvent further increases the production costs due to the necessary extra ventilation and filtration equipment for safety and protection standards.[12] Furthermore, NMP must undergo a recovery process after electrode processing, which makes the fabrication process with this solvent more expensive and complex.[10] Alternatively, water is used as the solvent to disperse aqueous-based binders, which are environmentally benign and almost four times cheaper than their organic counterpart. With all this, during the preparation of the electrode slurry, the cost of the PVDF dispersion in organic solvent (around 5\$/kg) is much higher than the dispersion of water-based binders (1\$/kg), such as the carboxymethyl cellulose (CMC) and styrene-butadiene rubber (SBR).[13] While the drying and solvent recovery system of NMP contribute to 3.4% of the battery pack costs,[14,15] not only there is no cost related with the solvent recovery for aqueous processing, but also the drying step is 4.5 times faster than for NMP and requires nearly 10 times less overall energy.[16] In fact, previous studies reported more airflow rate and higher temperature during the drying step for organic-based electrodes.[12,14] In addition, further savings for capital equipment purchasing can be generated with water-based electrode production since, unlike for combustible solvent NMP, it will not require explosion-proof slurry mixers.[13] All in all, turning from the classical organic processing route to the more environmentally friendly aqueous route can lead to a decrease of 80% in the electrode fabrication costs.[12] However, upscaling the aqueous processing technique for electrode fabrication is not as straightforward as one can imagine. Still, there are several drawbacks that need to be addressed, such as the presence of agglomerates of slurry components due to the strong interaction between colloidal particles,[17,18] Li dissolution,[19] transition metal leaching[20] and Al current collector corrosion.[21] Despite these difficulties, aqueous processing has been recently applied to manufacture LIB cathodes, including $LiCoO_2$ (LCO),[22] $LiNi_{0.33}Mn_{0.33}Co_{0.33}O_2$ (NMC111),[23] $LiNi_{0.5}Mn_{0.3}Co_{0.2}O_2$ (NMC532)[24] and $LiFePO_4$ (LFP).[25,26] In fact, the latter material has been processed following this route in the new cells from Tesla, Inc.[27,28] In addition, the use of water as the solvent is a widely implemented practice for the processing of state-of-the-art negative electrodes, such as graphite anodes.[29] While CMC or combination of CMC-SBR binders have already been successfully adapted and industrially adopted for anode slurry preparation,[11] aqueous processing for lithium transition metal oxides should be further investigated. Therefore, various researchers have recently driven their efforts towards the development of the aqueous processing of cathode electrodes. Such is the case of Chen et al.,[18] who used Na-CMC as a binder for the preparation of $LiNi_{0.4}Co_{0.2}Mn_{0.4}O_2$ electrodes that showed significantly better structural integrity compared with conventional organic PVDF-based electrodes. Moreover, these electrodes offered superior high rate capability as well as extremely stable cycling performance even

[z]E-mail: imeatza@cidetec.es

at elevated temperatures.[30] Loeffler et al.[31] demonstrated that high loading CMC-based cathodes could be successfully manufactured via aqueous processing. Then, the authors investigated the performance of balanced full cells with graphite anode in pouch cell configuration and obtained 2000 cycles with more than 70% of capacity retention.[31] Çetinel and Bauer investigated the effect of different amount of carbon black on the rheological properties and electrochemical performance of NMC111 with Na-CMC and fluorine acrylic hybrid latex (TRD 202A).[32,33] In fact, the addition of an acid is a practical solution to prevent corrosion of the aluminum foil due to the pH increase in the aqueous slurry. On the other hand, Azhari et al. reported intergranular cracking of NMC particles when exposed to water, which also led to lithium leaching.[34] In their work, they subjected NMC111, NMC622 ($LiNi_{0.6}Mn_{0.2}Co_{0.2}O_2$) and NMC811 ($LiNi_{0.8}Mn_{0.1}Co_{0.1}O_2$) to different exposure times to water under stirring. It was evident that the highest the nickel content of the layered oxide and the exposure period, the highest the negative impact of such exposure.

In this work, NMC622 has been processed following an aqueous route. Initially, an aqueous based formulation was developed at laboratory scale, in which the influence of different experimental parameters (such as the air convection, the pH neutralization or the drying temperature) on the quality of the electrodes were analyzed. Afterwards, the upscaling to a semi-industrial coating line is reported. This process is not trivial: the difficult adoption by industry of many of the advances reported by academia is being recurrently reported in critical reviews.[35] In some cases, the electrode processing methods, the materials used, or the physical characteristics of the slurry and the coating make it difficult to close the gap between fundamental research and industrial implementation.[36] The electrodes obtained in the coating line were tested in full coin cell (FCC) configuration using graphite-based counter electrodes. Furthermore, the performance of the cells using aqueous-based electrodes was compared with organic-processed electrodes. Interestingly, the capacity was significantly better retained with the former.

Experimental

Electrode preparation.—NMC622 (supplied by UMICORE) was used as the active material for the positive electrode. In aqueous formulations, polyvinylidene fluoride latex (PVDF, Kynar® RC-10,280, provided by ARKEMA) was used as a binder to maintain the structural integrity of the electrodes, the electric conductivity was enhanced by the addition of carbon black (C-NERGY Super C45 from IMERYS Graphite & Carbon), and battery-grade sodium carboxymethylcellulose (CMC, Walocel 2000 from DOW) as disperser and thickener to regulate the rheological behavior of the slurry. The weight fraction of the different components was 92% NMC622, 3% C45, 2% CMC and 3% PVDF. This formulation was used at both the laboratory scale, with 50 g total solid content and the electrode coating line with 500 g total solid content. The solid content in these slurries was 57%.

On the other hand, NMC622 was processed as well using N-methyl pyrrolidone (NMP, synthesis grade, Scharlab) as the solvent for the slurry. In this case, C-NERGY Super C65 from IMERYS Graphite & Carbon and Kynarflex© LBG PVDF from ARKEMA were used as the conductive additive and the binder, respectively. The weight fraction of the components was 92% NMC622, 3% C45 and 5% PVDF. This organic-processed electrode was only prepared at CIDETEC's electrode coating line. The solid ratio in organic slurry was 54%.

Anodes were prepared using water as solvent. They consisted of 94% graphite (Hitachi HE3), 2% C45, 2% CMC and 2% Styrene-Butadiene Rubber (SBR, BM451B, ZEON) and were manufactured in a continuous coating line (Coatema GmbH, Basecoater) with a knife coating system at CIDETEC. The slurry consisted of 4.5 kg solids with a solid to liquid ratio of 1/0.8.

Laboratory scale cathode slurry (prepared by aqueous route, prior to the upscaling to the coating line) was casted using a table-top doctor blade onto 20 μm-thick aluminum (Hydro) foil. The target loading of the cathode was 3.0 mAh cm^{-2}. Water was evaporated by introducing the coatings in an oven at different temperatures (discussed in the Results and Discussion section). Afterwards, the cathodes were calendered to 3.0 g cm^{-3} (~35% porosity) using a table-top calender-machine (DPM solutions). The thickness of the coatings was measured using a Mitutoyo 389–271C micrometer.

Cathode coatings prepared at CIDETEC's coating line were elaborated using a C-coated aluminum foil (15 μm-thick, GELON). The reason behind this difference with respect to laboratory-scale cathodes is detailed in the Supplementary Information (Figs. S1 and S2). 8 μm-thick Cu current collector (Furukawa) was used for the anode. The electrolyte was evaporated from the coating by going through three consecutive convection ovens (3 meters total). The temperatures of these three consecutive ovens were 50 °C, 60 °C and 70 °C for the evaporation of water, while to evaporate NMP they were adjusted to 105 °C, 115 °C and 120 °C. The areal loading of the cathodes and the anode were 3.0 and 3.3 mAh cm^{-2}, respectively. Cathodes were densified to 3.0 g cm^{-3} and anodes to 1.4 g cm^{-3} (~35% porosity) using a semi-industrial calendaring machine (LDHY 400-N45, Naknor).

Before doing the coatings, the rheological behavior of the slurries was characterized. For that aim, three fractions (~10 ml each) of the corresponding slurry were analyzed in a DHR2 rheometer from TA instruments. Furthermore, the adhesion strength of the coated electrodes on the current collector was measured using the 90° peel test (LS1 model, Lloyd Instrument) on 3 stripes of 2 cm width. The correct dispersion of the different components in the coatings was analyzed by means of field emission scanning electron microscope (FE-SEM, ULTRA plus ZEISS). Finally, the water traces in the electrodes were determined by Karl-Fischer titration (Titroline KF Trace M3, Schott Instruments) with equipment installed inside the dry room, where the cells were assembled.

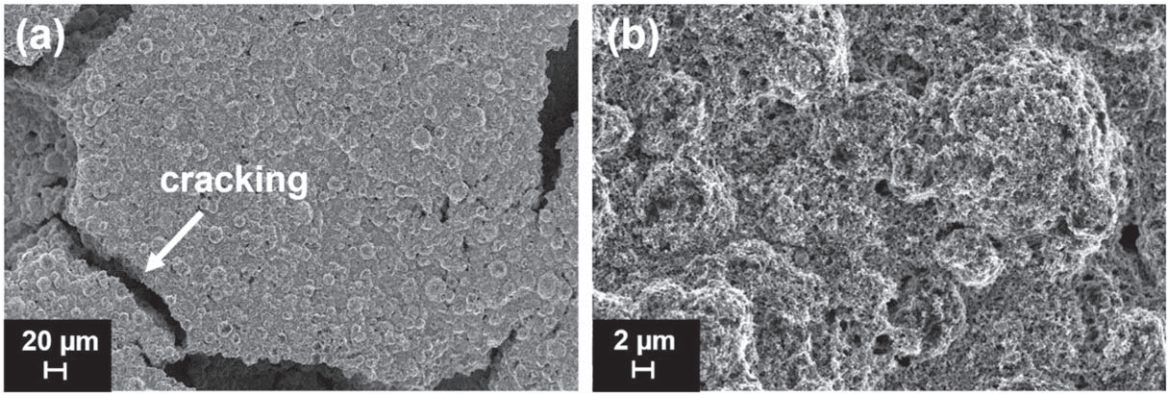

Figure 1. FE-SEM images of as-coated aqueous cathode layer surface with a magnification of (a) x500 and (b) x5000.

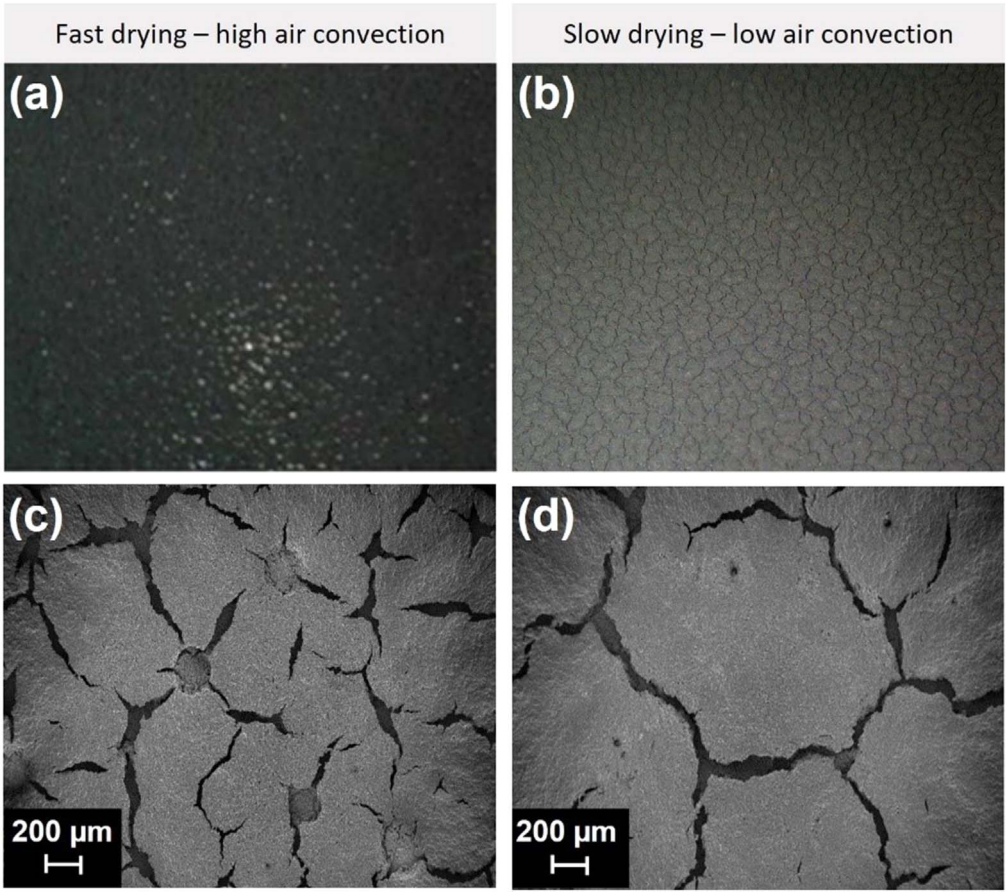

Figure 2. Cathode morphology issues observed on aqueous slurries. (a) Optical images of as-coated cathode layer surface in conventional "fast" drying conditions and (b) under low-convection slow drying. Corresponding FE-SEM images: cathodes dried under (c) high and (d) low air convection.

Electrochemical cell.—Coatings were cut into disks with a diameter of 16.6 mm (working electrodes) and 17.7 mm (counter electrodes) and dried overnight under vacuum in a dry room to eliminate the water traces before cell assembly. Anodes were dried at 120 °C, while the drying temperature of the cathodes is analyzed in this work. The cell cases were cleaned with ethanol in an ultrasonic bath for 15 min and dried at 60 °C for 1 h. On the other hand, a lithium foil ($\varnothing$ = 18.2 mm, 50 μm thickness, from Albemarle) was used as counter and reference electrode in half coin cell (HCC) configuration. The coin cells were assembled using Celgard 2500 separator ($\varnothing$ = 18.92 mm) with 75 μl of electrolyte. The electrolyte for HCCs was 1 mol l^{-1} lithium hexafluorophosphate in (3:7 vol%) ethylene carbonate: ethyl methyl carbonate + 2 wt% fluoroethylene carbonate (1 M $LiPF_6$ in EC:EMC (3:7) + 2% FEC, from ARKEMA). Besides, full coin cells (FCCs) were assembled using 1 mol l^{-1} lithium hexafluorophosphate in (1:1 vol%) ethylene carbonate: dimethyl carbonate + 2 wt% vinylene carbonate (1 M $LiPF_6$ in EC:DMC (1:1) + 2% VC, from Solvionic) as electrolyte. 75 μl of this electrolyte were added in the Celgard 2500 separator. Coin cells (CR2025, Hohsen) were assembled inside the dry room (−50 °C dew point). Electrodes were balanced for a negative/positive ratio of 10% of excess of capacity in the negative electrode. Three cells per experiment were assembled.

Electrochemical testing.—After assembly, coin cells were tested in a Basytec Cell Test System potentiostat at 25 °C ± 1 °C controlled by air conditioning. Cells were kept at open circuit for 16 h to ensure the proper wetting of the separator and the electrode pores with the electrolyte. Formation of HCCs and FCCs with graphite anode consisted of three C/10 cycles. Afterwards, brief rate capability tests were conducted by performing galvanostatic cycles at C/2, 1C, C/2, 2C and C/2. Finally, cells were subjected to 1C cycle life test until 80% of state of health (SOH) was reached. The galvanostatic cycles of FCCs were performed between 2.8 and 4.3 V, while the potential range selected for HCCs was 2.7 V–4.45 V. All the charges were conducted at C/3 and included a constant voltage step to C/10.

Post-mortem characterization.—After reaching 80% SOH, the cells were transferred to an MBraun glovebox and disassembled inside ($[O_2] < 0.1$ ppm, $[H_2O] < 0.5$ ppm). The salts deposited onto the electrodes were removed by washing in dimethyl carbonate. Afterwards, the crystal structure of the electrodes after the electrochemical experiments was analyzed by means of powder X-ray diffraction (XRD), using a Bruker D8 Discover diffractometer (Cu Kα radiation, λ = 0.154 nm) equipped with a LynxEye PSD detector. The diffractograms were recorded between $2\theta = 10°$ and 85° at 0.003° s^{-1}, while the obtained data were fitted using the FULLPROF program.[37] In addition, the electrodes were also subjected to FE-SEM analysis.

Results and Discussion

Lab-scale aqueous processing and characterization of the cathodes.— *Slurry preparation and coating conditions.*—Slurry rheology, morphology (by FE-SEM) and adhesion of the coated layer to the current collector as well as electrochemical performance were analyzed for the lab-scale aqueous processed cathodes. The aim of such experiments was to obtain preliminary information on the electrode preparation parameters prior to upscaling to pilot plant-scale coater. The waterborne slurry formulation showed appropriate slurry homogeneity, stability and shear thinning behavior after adjustment of slurry mixing steps: C45 carbon black was initially dispersed in the CMC solution with subsequent addition of the

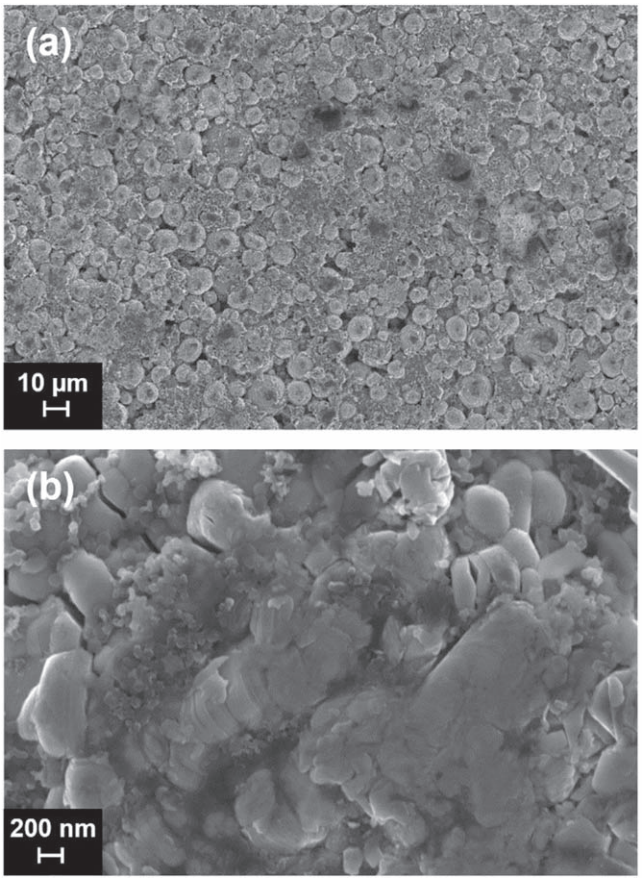

Figure 3. Top-view FE-SEM images of the surface of the water-processed NMC622 electrode calendered at 120 °C and further died under vacuum at 140 °C for 16 h. (a) x1000 and (b) x5000 magnification.

NMC622 and binder latex. Although the pH of the aqueous slurry was below 12, it was still measured around 11.3–11.9. This basic pH may cause metal leaching from the NMC active material and Al current collector corrosion, both phenomena being detrimental for the electrochemical performance of water-processed NMC cathodes.

Another key point observed on aqueous processing of these NMC622 cathodes was the high thickness of the cathode layer casted from these aqueous slurries. For the same loading, as coated layers from aqueous slurries of 50% solids content were up to 80% thicker than from conventional organic processing. Moreover, cracking was observed on the dry layer caused during solvent evaporation Fig. 1.

Cracking in high-loading water-processed NMC electrodes is a drawback that is not that frequently observed in analogous NMP-processed electrodes.[19] In order to address this issue, the drying temperature was changed between 80 °C and 60 °C, as well as the drying time and convection flux effect in the oven used at lab-scale. The change in drying temperature did not yield any difference on the appearance of cracks and defects on drying, whereas the convection flux seemed to have an impact. As shown in Fig. 2, while fast drying in 10 min and with high convection promoted the formation of many cracks and even circular defects indicative of bubble evaporation (Figs. 2a and 2c), lower convection and slow drying reduced the degree of cracking (Figs. 2b and 2d). Furthermore, observing the reduction in dry thickness of electrodes positioned on shelves further away from the convection oven fan seemed to link the thickness and higher porosity with a more intense air convection flux accelerating water evaporation. Although cracks could be minimized by drying at 60 °C and without convection in the oven, they could not be fully eliminated.

The research on cathode processing, and particularly on solving the cracking issues, continued by measuring the pH of slurries to control the risk of Al corrosion with H_2 gas formation and metal leaching from the active material. In this regard, NMC622 showed high pH in aqueous suspension (10.89 initial and 10.92 after stirring for 4 h), which involves risk of Al corrosion. Therefore, diluted phosphoric acid solution was used as pH buffer and control of the final slurry at pH ≤ 9. Even if the viscosity of the slurry was slightly increased, this addition did not show any significant effect on the slurry rheology (Fig. S3). After lab-scale coating and drying at 60 °C and low air convection flux, the thickness of the as-coated electrode layers was reduced to the same range as for NMP-based electrodes. There was no gas or bubble formation during solvent evaporation and cracks were eliminated.

The slurry with diluted phosphoric acid addition to maintain the slurry pH at ∼8 was applied and calendered afterwards at high temperature - 120 °C - to activate (melt) de PVDF, in a lab-scale roll pressing machine with heated rolls. The morphology of the electrodes was homogeneous but on higher magnifications in FE-SEM (Fig. 3), some areas with C45 agglomeration as well as unmelted PVDF could still be observed. Additionally, microcracks on the secondary particles of the NMC622 active material could be detected after calendering to the target density. Furthermore, even after subsequent vacuum drying for 16 h before cell assembly, at temperatures near the melting temperature of the PVDF (120 °C), a degree of unmelt PVDF spherical particles could be observed. Adhesion strength measured by 90° peel test showed improved

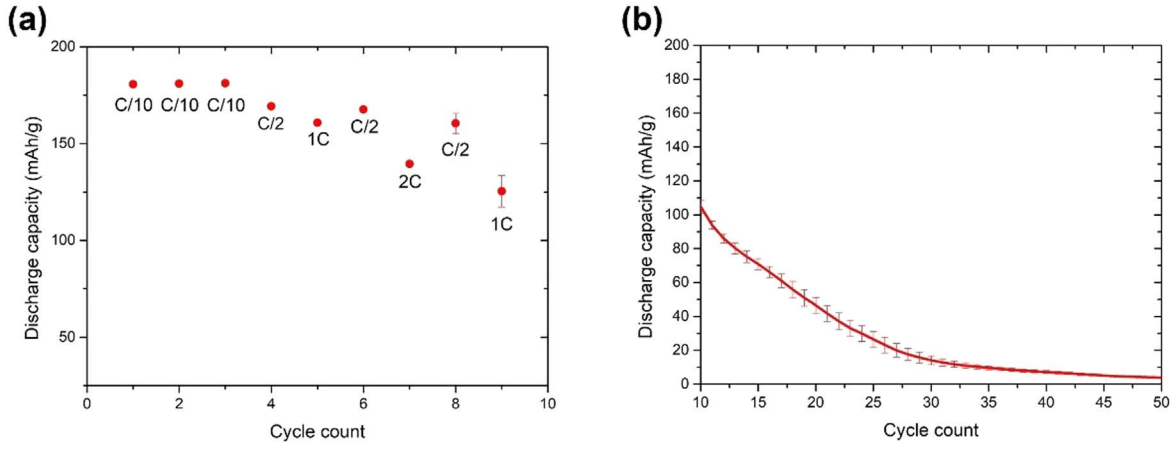

Figure 4. Electrochemical performance of aqueous processed cathodes: (a) rate-capability tests and (b) galvanostatic cycling at 1C discharge—C/3 charge C-rates.

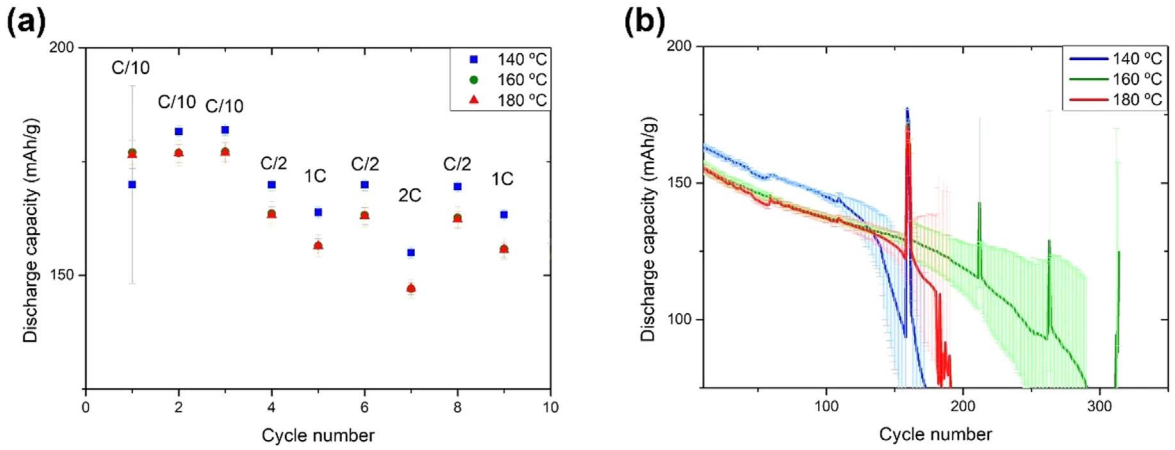

Figure 5. (a) Rate capability and (b) 1C galvanostatic cycling tests conducted on HCCs dried at 140 (blue squares, line), 160 (green circles, line) and 180 °C (red triangles, line).

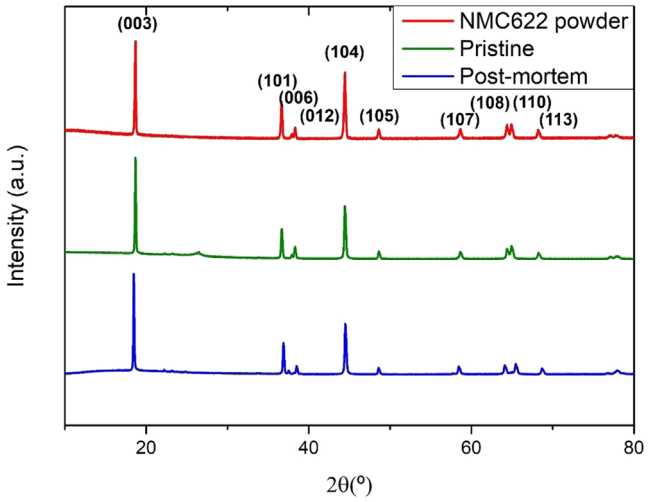

Figure 6. X-ray diffraction patterns of the NMC622 powder (red line), the pristine NMC622 coating (green line) and the post-mortem electrode (blue line).

results for calendered electrodes, with 16 N m^{-1} and up to 19 N m^{-1} after vacuum drying.

To complete the characterization before upscaling, peel tests of cathodes after soaking (in DMC at 30 °C) were performed to evaluate swelling and mechanical stability of the cathode in contact with electrolyte. No relevant change in weight of sample after soaking could be measured and thickness variation related to swelling was not observed for 15 h soaking. However, the sample swelled after 24 h soaking, with up to +5% thickness increase.

Electrochemical testing in HCCs and analysis of drying temperature.—Cathodes at target loading 3.0 mAh cm^{-2} and density 3 g cm^{-3} were validated in half coin cells prior to upscaling the electrode manufacturing to the pilot scale coating line. The cell consisting of aqueous-processed NMC622 provided 180 mAh/g_{NMC622} at 0.1C discharge C-rate Fig. 4.

At highest discharge C-rate of 2C, the cells provided outstanding performance with 140 mAh g^{-1} (Fig 4a). However, during subsequent cycling (Fig. 4b), a very fast and drastic drop of capacity was observed, yielding close to zero capacity after a few cycles. This capacity fade was attributed to Li electrode degradation and/or electrolyte consumption; these cells were opened inside an Ar-filled glove box to perform the visual inspection of the cells. This inspection revealed that the cells were dry, and the color of the remaining lithium electrode was dark grey, evidencing its degradation. Some pictures of the cell-opening are shown in Fig. S4.

In this context, vacuum drying at higher temperatures was explored to decrease the residual water content that may otherwise get released and react detrimentally with the electrolyte and Li foil during cell operation. In fact, high water content was measured by Karl-Fischer titration method (set up in −50 °C dew point dry room) on the aqueous processed cathodes after standard vacuum drying for 16 h at 120 °C: 1110 ppm H_2O. The Karl-Fischer measurement revealed a decrease of the residual water content in the electrode with the increase of the vacuum drying temperature (Table SI). Beyond 160 °C and particularly at 180 °C, water content measured was lower than 500 ppm.

Rate capability and galvanostatic cycling tests at 1C–0.5C discharge-charge C-rates were conducted in HCC configuration to evaluate the influence of electrode vacuum drying temperature on the electrochemical performance. Results are shown in Fig. 5. Rate capability experiments (Fig. 5a) evidenced that the electrodes dried at 140 °C provided higher discharge capacity than those dried at higher temperatures. Indeed, this capacity was higher for all their cycle life which, on the other hand, was shorter than for the rest of the cells (Fig. 5b). This was attributed to the presence of water in the redox activity of these cells, which could accelerate the capacity fade of the cells. Besides, electrodes dried at 160 and 180 °C showed quite a reproducible performance, with similar capacities on both the rate capability experiments and the beginning of the cycling performance tests. Capacity fade of cells dried at 180 °C, however, showed an irregular behavior with large error bars (corresponding to the standard deviation between the different samples) starting from cycle 175. This is attributed to the different behavior of the three cells dried at 180 °C: while two of them underwent capacity fade after 175 cycles (and provided almost 0 mAh g^{-1} between 175 and 250 cycles), there was still one cell cycling efficiently, which elevated the average capacity value. All in all, the cells providing the better capacity retention were those dried at 160 °C. Furthermore, regardless the drying temperature selected (i.e., 140, 160 or 180 °C), the cycle performance of the cells was improved when compared with the original drying temperature (120 °C).

Post-mortem characterization.—The cathodes from the disassembled cells were washed with DMC and subjected to post-mortem analysis, studying their morphology by FE-SEM and the structural changes in NMC622 phases (different degree of lithiation and/or possible degradation in MO_x oxides) by X-ray diffraction (XRD).

The morphology observed on the harvested cathodes, as shown in Fig. S5, differed only slightly from the pristine uncycled samples: a thin film covering the surface may be distinguished - likely related to CEI (Cathode Electrode Interface) film formation—as well as

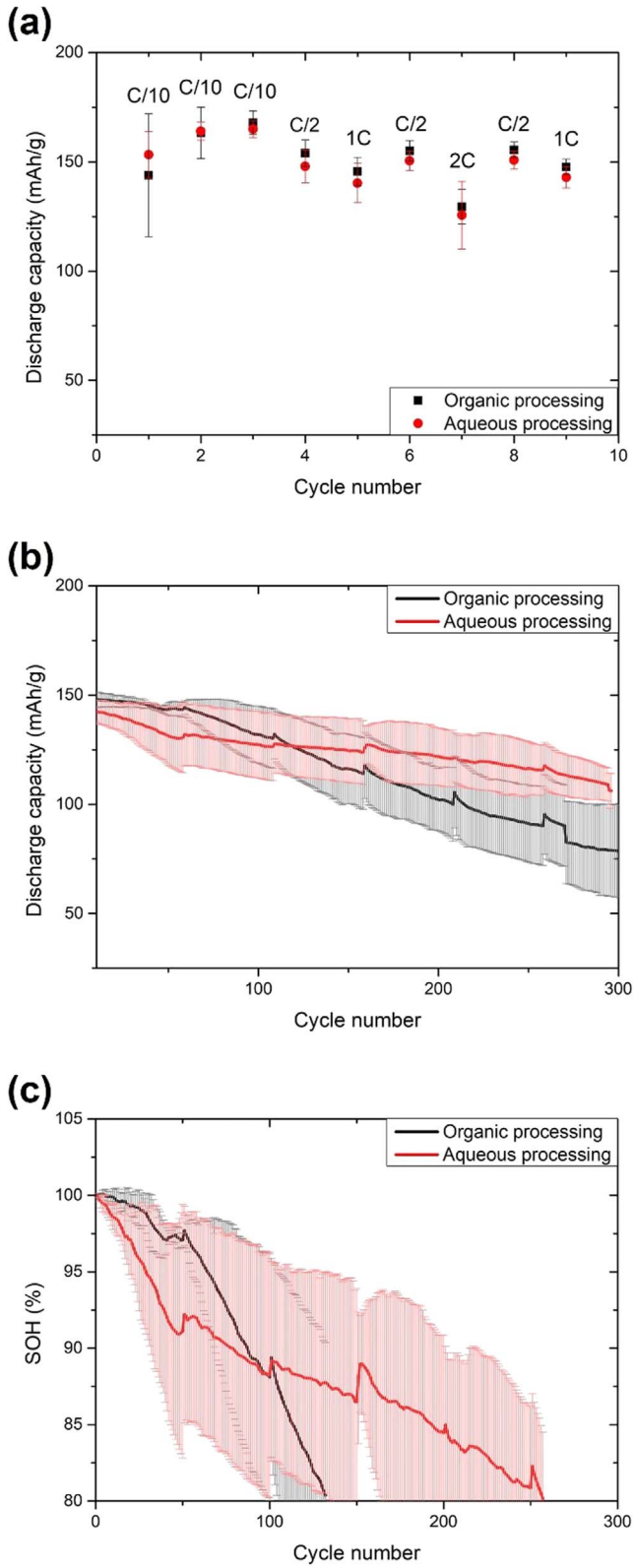

Figure 7. Evolution of the discharge capacity in (a) rate capability (b) 1C cycle life tests and (C) SOH evolution upon cycling of FCCs consisting of organic (black) and water-processed (red) cathodes and graphite anodes cycled between 4.3 and 2.8 V.

needle-like structures revealed in the NMC622 spherical particles upon cycling in the FE-SEM cross-sections. Nevertheless, no mayor porosity occlusion nor particle detachment were detected.

The NMC622 powder, the pristine coating and a cycled electrode were subjected to the analysis by XRD. The diffractograms obtained are shown in Fig. 6. The diffractograms were fitted using the R −3 m hexagonal space group (JCPDS No. 00–85–1968, $Li_{0.89}Ni_{1.01}O_2$).[38,39] The fitted spectra and the unit cell parameters can be found in Fig. S6 and Table SII, respectively. All the diffractograms have their maximum at $2\theta \sim 18.5°$, corresponding to the (003) diffraction peak of NMC.[40] The comparison between the diffractograms of the NMC622 and the pristine NMC622 coating reveal negligible differences in the signals associated with NMC622. In fact, the unit cell parameters were almost identical (see Table SII for further detail), suggesting negligible structural modifications of NMC622 during the aqueous processing of the material. Nevertheless, an additional reflection at $2\theta = 26.3°$ was obtained for the pristine coating, which was ascribed to the graphite fraction in the carbon black used to enhance the electrical conductivity of the electrode (R −3 m, hexagonal, JCPDS No. 01–73–5918).[38] In addition, two negligible features appeared at $2\theta = 22.3°$ and 23.3°, whose identity remains unsolved. Furthermore, these signals were observed as well in the post-mortem electrode. In the latter, the contribution of carbon could not be observed in the diffractogram. However, there were slight variations in the diffraction pattern when the pristine and cycled electrode were compared. The most significant difference was the shift of the (003) peak to smaller angles, which is usually associated with a different degree of lithiation. The results of the fitting were in good agreement with this hypothesis, evidencing a decrease in the unit cell parameters of the post-mortem NMC622 electrode. Before the electrochemical experiments are performed, NMC622 is fully lithiated and therefore, the unit cell is fully expanded. After several discharge-charge cycles, some lithium is consumed (in processes such as the SEI formation) and, thus, NMC does not recover its fully-lithiated state. More interestingly, no additional phases were found in the diffractogram of the cycled NMC622 electrode, evidencing its stability towards successive lithiation-delithiation cycles.

Upscaling to coating line and electrochemical testing in FCC.—After completing the characterization of the electrodes elaborated at laboratory-scale, the recipe was upscaled to CIDETEC's semi-industrial electrode manufacturing line. Upscaling was not simple, and delamination was observed when the same current collector as in laboratory-scale coatings was used. This inconvenience was overcome by using carbon-coated current collector, as detailed in Supplementary Information (Figs. S1 and S2). Finally, the electrochemical validation of the cathodes prepared at the electrode manufacturing line was conducted in FCC configuration. For this aim, cells were assembled vs. negative electrodes consisting of graphite as the active material. Additional cells consisting of NMC622 cathodes prepared using organic solvent were tested for directly evaluating the performance of the water-processed NMC622 cathodes. The comparison of the results of the cells assembled with graphite anodes vs water- and organic-processed NMC622 cathodes are shown in Fig. 7. The cells were subjected to a cycling protocol consisting in an initial rate capability experiment (Fig 7a) followed by cycling at 1C–0.5C discharge-charge C-rate block, including a 0.1C recovery cycle every 50 cycles (Figs. 7b, 7c). Galvanostatic profiles of the selected cycles were included in Supplementary Information (Fig. S7), where a higher polarization was not observed in full cells with aqueous-processed electrodes, contrary to other works with aqueous-processed NMC622.[41] The rate capability results obtained with both types of cathodes were very similar (Fig. 7a). The capacity in the first cycles was higher for the water-processed electrodes, in good agreement with Hoffman et al.[21] Regarding the 1C cycling tests (Fig. 7b), the cells with water-processed cathodes provided an average initial discharge capacity slightly lower than those processed using organic solvent (143 and 148 mAh g^{-1} for the former and the latter, respectively). This could be attributed to lithium leaching during the water processing of NMC.[21] The capacity retention, however,

was significantly higher with the water-processed electrodes; they completed 265 cycles before reaching the 80% of SOH, while the cells based on NMP-based electrodes reached this limit after 140 cycles. Besides, it is worth mentioning that the capacity retention observed in FCCs was significantly higher than in HCCs and, therefore, the early capacity fade of the latter can be attributed to the lithium electrode.

Conclusions

In this work, NMC622 cathodes were prepared at laboratory scale and upscaled to electrode manufacturing line following an aqueous route. Different processing parameters affecting the performance of the electrodes were studied. It was observed that drying of coating at low air convection flux improved the electrode quality but could not be transferred to electrode production, while 160 °C was determined as the best vacuum drying temperature for the electrodes before assembling electrochemical cells. In any case, the cracking caused by the higher aqueous-electrode thickness compared to organic processing could not be fully overcome by the coating drying conditions but can be significantly mitigated by the addition of phosphoric acid as pH buffer, avoiding Al corrosion and H_2 bubble generation. The electrodes tested in HCC configuration were subjected to post-mortem evidencing high stability. Laboratory-scale recipe was upscaled to a semi-industrial electrode coating line and the electrodes obtained were subjected to electrochemical validation in FCCs using graphite as negative electrode. Interestingly, the performance of water-processed cathodes surpassed that of organic-processed NMC622. The work described in this article shows the importance of controlling different aspects and parameters of the electrode processing prior to upscaling to industrial coating line. Furthermore, the appearance of new unexpected drawbacks evidence that upscaling is not a trivial step in electrode manufacturing. In any case, waterborne electrodes outperformed those prepared following the state-of-the-art NMP-based processing.

Acknowledgments

This work has received funding from the European Union's Horizon 2020 research and innovation programme under grant agreements No 769929 (IMAGE) and No 814464 (Si-DRIVE). The authors gratefully acknowledge UMICORE (Pierre-Etienne Cabelguen) for the NMC622 cathode active material and ARKEMA (Stéphane Bizet) for the PVdF waterborne latex and electrolyte supply and fruitful discussion. We would also like to thank Carmen Palacios, Iñigo Arzac and Andoni Contreras from CIDETEC for the SEM measurements and for the manufacturing of the electrodes.

ORCID

Iratxe de Meatza https://orcid.org/0000-0001-8245-5815
Imanol Landa-Medrano https://orcid.org/0000-0003-4180-5262
Susan Sananes-Israel https://orcid.org/0000-0002-0580-0627
Verónica Palomares https://orcid.org/0000-0002-3269-8656

References

1. C. P. Grey and D. S. Hall, *Nat. Commun.*, **11**, 2 (2020).
2. D. Liu, H. Wang, Y. Peng, W. Xie, and H. Liao, *Energies*, **6**, 3654 (2013).
3. F. Wu, J. Maier, and Y. Yu, *Chem. Soc. Rev.*, **49**, 1569 (2020).
4. A. Manthiram, *ACS Cent Sci*, **3**, 1063 (2017).
5. A. Masias, J. Marcicki, and W. A. Paxton, *ACS Energy Lett.*, **6**, 621 (2021).
6. G. Pistoia and B. Liaw, "Behaviour of Lithium-Ion Batteries in Electric Vehicles: Battery Health, Performance, Safety, and Cost." (Berlin)(Springer) 1st ed., p 344 (2018), https://link.springer.com/book/10.1007/978-3-319-69950-9.
7. F. T. Wagner, B. Lakshmanan, and M. F. Mathias, *J. Phys. Chem. Lett.*, **1**, 2204 (2010).
8. Y. Ding, Z. P. Cano, A. Yu, J. Lu, and Z. Chen, *Electrochemical Energy Reviews*, **2**, 1 (2019).
9. P. Liu, R. Ross, and A. Newman, *MRS Energy & Sustainability*, **2**, 1 (2015).
10. S. N. Bryntesen et al., *Energies*, **14**, 1406 (2021).
11. D. Bresser, D. Buchholz, A. Moretti, A. Varzi, and S. Passerini, *Energy Environ. Sci.*, **11**, 3096 (2018).
12. D. L. Wood, J. Li, and C. Daniel, *J. Power Sources*, **275**, 234 (2015).
13. R. Demiryürek et al., *Int. J. Energy Res.*, **45**, 21182 (2021).
14. D. L. Wood et al., *Drying Technol.*, **36**, 234 (2018).
15. S. Ahmed, P. A. Nelson, K. G. Gallagher, and D. W. Dees, *J. Power Sources*, **322**, 169 (2016).
16. N. Susarla, S. Ahmed, and D. W. Dees, *J. Power Sources*, **378**, 660 (2018).
17. J. Li et al., *JOM*, **69**, 1484 (2017).
18. J. Li, B. L. Armstrong, C. Daniel, J. Kiggans, and D. L. Wood, *J. Colloid Interface Sci.*, **405**, 118 (2013).
19. R. Sahore et al., *ACS Sustain Chem Eng*, **8**, 3162 (2020).
20. M. Wood et al., *Energy Storage Mater.*, **24**, 188 (2020).
21. M. Hofmann, M. Kapuschinski, U. Guntow, and G. A. Giffin, *J. Electrochem. Soc.*, **167**, 140535 (2020).
22. J. T. Lee, Y. J. Chu, F. M. Wang, C. R. Yang, and C. C. Li, *J. Mater. Sci.*, **42**, 10118 (2007).
23. N. Loeffler et al., *ChemSusChem*, **10**, 3581 (2017).
24. Z. Du et al., *J. Power Sources*, **354**, 200 (2017).
25. J. Li, B. L. Armstrong, J. Kiggans, C. Daniel, and D. L. Wood, *J. Electrochem. Soc.*, **160**, A201 (2013).
26. A. Kvasha et al., *Electrochim. Acta*, **215**, 238 (2016).
27. G. H. Ruffo, (2020), 446245 https://insideevs.com/news/446245/tesla-slide-25000-car-lfp-batteries/.
28. S. Alvarez, *Elon Musk's Tesla Model 3 cobalt-free strategy is ushering in an LFP battery movement* (2021).
29. A. A. Tidblad et al., *Energies*, **14**, 4223 (2021).
30. Z. Chen et al., *J. Power Sources*, **372**, 180 (2017).
31. N. Loeffler et al., *J. Power Sources*, **248**, 915 (2014).
32. F. A. Çetinel and W. Bauer, *Bull. Mater. Sci.*, **37**, 1685 (2014).
33. W. Bauer, F. A. Çetinel, M. Müller, and U. Kaufmann, *Electrochim. Acta*, **317**, 112 (2019).
34. L. Azhari et al., *ACS Appl. Mater. Interfaces*, **12**, 57963 (2020).
35. Y. Liu, R. Zhang, J. Wang, and Y. Wang, *iScience*, **24**, 102332 (2021).
36. M. Ue, K. Sakaushi, and K. Uosaki, *Mater. Horiz.*, **7**, 1937 (2020).
37. J. Rodríguez-Carvajal, *Physica B: Physics of Condensed Matter*, **192**, 55 (1993).
38. I. Landa-Medrano et al., *J. Electrochem. Soc.*, **167**, 090528 (2020).
39. D. Müller et al., *Electrochim. Acta*, **391**, 138966 (2021).
40. Q. Wang et al., *ACS Appl. Mater. Interfaces*, **9**, 24731 (2017).
41. D. Pritzl et al., *J. Electrochem. Soc.*, **166**, A4056 (2019).